References and Notes

1. A. Fire *et al*., *Nature* **391**, 806 (1998).
2. S. M. Hammond, A. A. Caudy, G. J. Hannon, *Nature Rev. Genet.* **2**, 110 (2001).
3. A. J. Hamilton, D. C. Baulcombe, *Science* **286**, 950 (1999).
4. P. D. Zamore, T. Tuschl, P. A. Sharp, D. P. Bartel, *Cell* **101**, 25 (2000).
5. S. M. Hammond, E. Bernstein, D. Beach, G. J. Hannon, *Nature* **404**, 293 (2000).
6. R. F. Ketting, T. H. Haverkamp, H. G. van Luenen, R. H. Plasterk, *Cell* **99**, 133 (1999).
7. C. Cogoni, G. Macino, *Science* **286**, 2342 (1999).
8. T. Dalmay, R. Horsefield, T. H. Braunstein, D. C. Baulcombe, *EMBO J.* **20**, 2069 (2001).
9. D. Wu-Scharf, B. Jeong, C. Zhang, H. Cerutti, *Science* **290**, 1159 (2000).
10. A. Smardon *et al*., *Curr. Biol.* **10**, 169 (2000).
11. C. Cogoni, G. Macino, *Nature* **399**, 166 (1999).
12. T. Dalmay, A. Hamilton, S. Rudd, S. Angell, D. C. Baulcombe, *Cell* **101**, 543 (2000).
13. P. Mourrain *et al*., *Cell* **101**, 533 (2000).
14. H. Tabara *et al*., *Cell* **99**, 123 (1999).
15. C. Catalanotto, G. Azzalin, G. Macino, C. Cogoni, *Nature* **404**, 245 (2000).
16. M. Fagard, S. Boutet, J. B. Morel, C. Bellini, H. Vaucheret, *Proc. Natl. Acad. Sci. U.S.A.* **97**, 11650 (2000).
17. T. Tuschl, P. D. Zamore, R. Lehmann, D. P. Bartel, P. A. Sharp, *Genes Dev.* **13**, 3191 (1999).
18. E. Bernstein, A. A. Caudy, S. M. Hammond, G. J. Hannon, *Nature* **409**, 363 (2001).
19. R. F. Ketting *et al*., in preparation.
20. J. C. Clemens *et al*., *Proc. Natl. Acad. Sci. U.S.A.* **97**, 6499 (2000).
21. S2 cells were soaked with luciferase dsRNA at 3 mg/liter and harvested after 7 days. Hypotonic extracts were spun at 200,000*g* for 3 hours to pellet ribosomes, which were resuspended and extracted in 400 mM potassium acetate (KOAc). Resultant soluble protein was precipitated by 1:4 dilution in hypotonic buffer and redissolved in buffer A [20 mM Hepes (pH 7.0), 2 mM $MgCl_2$, 2 mM dithiothreitol, and 0.5% octyl glucoside] with 400 mM KOAc. This protein was then fractionated on Superose-6 HR10/10 (Pharmacia). Fractions were assayed for RISC activity as described (*5*). The fraction showing peak activity was diluted 1:5 in buffer A and fractionated over a Mono S HR5/5 column (Pharmacia) with a linear gradient elution of buffer A with 0 to 500 mM KCl. The RISC fraction with peak activity from the Mono S column was then fractionated on a Mono Q HR5/5 column (Pharmacia); in turn, the active RISC fraction from this column was fractionated on hydroxyapatite HT (Bio-Rad) in a HR5/5 column (Pharmacia). Elution was in buffer A with 400 mM KCl, with a gradient of KH_2PO_4 from 0 to 500 mM. Fractions were analyzed on a 10% polyacrylamide gel. Four bands appeared to cofractionate with the active RISC fraction and were excised for microsequencing. Total protein was reduced by a factor of 10^6 during the entire purification. The estimated purification was 1:10,000.
22. Protein bands were digested with modified trypsin (Roche) and analyzed by liquid chromatography–mass spectrometry (LCQ MS/MS; Hewlett-Packard HP1100 connected to a Thermo-Finnigan LCQdeca electrospray ionization ion trap mass spectrometer). The acquired MS data were analyzed by SEQUEST software (Thermo-Finnigan) against the National Center for Biotechnology Information (NCBI) database.
23. Polyadenylated RNA was obtained from S2 cells and *Drosophila* 0- to 12-hour embryos using Trizol (Gibco) followed by magnetic oligo(dT) bead selection (Dynal); 2.5 μg of RNA from each source was used to construct a λZAP cDNA library using a commercial kit (Stratagene). This library was screened using a PCR probe corresponding to nucleotides 811 to 1069 in the GenBank predicted coding sequence. Two of four clones were full length; however, one had four missing NH_2-terminal polyglutamine repeats.
24. Total RNA from S2 cells, *Drosophila* 0- to 12-hour embryos, and adult whole body was fractionated on 1% agarose formaldehyde gel and transferred to Hybond N+ (Pharmacia). The membrane was hybridized with a ^{32}P-labeled oligonucleotide, CTGAGGCGGTAATGGTAATGGGGCAGCCTGCTGTTGCTGAGGTGGTCCAC.
25. PCR was done using 1 μg of S2 genomic DNA, first-strand cDNA prepared using the *C. thermus* kit (Roche), 0.001 ng of the full-length λZAP clone, or 0.001 ng of ago2/pIZ expression construct as templates. Primers were AACAGCAGGTACAAGGGTGGA and GATTGGTATTGGCCTTGGCTC. Roche taq conditions were used for 45 cycles.
26. A peptide corresponding to the eight COOH-terminal amino acids of AGO2 was conjugated to KLH and used for inoculation into rabbits for polyclonal antibody production (Covance). Antibodies were affinity-purified on a peptide-conjugated resin (Sulfolink, Pierce Biochemicals).
27. Ago2 was amplified with the primers ACCGATATCACCATGGCTAGTATGACTGGTGGTCAACAAATGGGTCACCATCACCATCATCACATGCCTTCTGTGGCATACCAC and ACCCTCGAGTCAGACAAAGTACATGGGGGT. This initiates at the second methionine codon, truncating the polyglutamine tract. The product was cloned into the expression vector pIZ (Invitrogen). S2 cells were transfected with 15 μg of luciferase dsRNA and 45 μg of ago2/pIZ per 15-cm plate, as described. Hypotonic extracts were made, adjusted to 400 mM KOAc, 0.5% octyl glucoside, and loaded on 1 ml of talon resin (Clontech) in a hi trap column (Pharmacia). Protein was eluted with an imidazole gradient, 0 to 100 mM, 10 column volumes. Protein was analyzed by Western blotting using T7 antiserum (Novagen). RNA was extracted with trizol and run on 15% acrylamide/urea/tris-acetate-EDTA gel. RNA was electroblotted as described and membranes probed with luciferase sense riboprobe (*5*).
28. S. M. Hammond, S. Boettcher, A. A. Caudy, R. Kobayashi, G. J. Hannon, data not shown.
29. *Drosophila* S2 cells were incubated with dsRNA (30 mg/liter) corresponding to either the first 500 nt of GFP or the first or last ~1000 nt of *AGO2* for 30 min in the absence of serum (*20*). Serum was added to a final concentration of 10%, and cells were cultured in suspension for 48 hours at 27°C. Cells were then divided into six-well dishes and cotransfected with a combination of *Renilla* and firefly luciferase expression vectors (3 μg total) and with dsRNA corresponding either to a control (GFP) or to firefly luciferase (75 ng). Assays for Firefly and *Renilla* luciferase were performed 36 hours after transfection. All analyses were performed on triplicate transfections. Identical experiments were also performed with *Renilla* dsRNA with a qualitatively similar outcome. For Western blotting, aliquots of soaked cells were lysed directly in SDS sample loading buffer.
30. S2 cells were transfected with a vector that directs the expression of a T7 epitope–tagged Dicer protein (*18*) or with a control vector. Cells were lysed and Dicer protein was immunoprecipitated as described (*18*). Proteins were released from Protein A–Sepharose beads by boiling in SDS sample loading buffer and were analyzed by Western blotting with the affinity-purified AGO2 antibody.
31. K. Bohmert *et al*., *EMBO J.* **17**, 170 (1998).
32. Y. Kataoka, M. Takeichi, T. Uemura, *Genes Cells* **6**, 313 (2001).
33. A. Grishok *et al*., *Cell* **106**, 23 (2001).
34. G. Hutvágner *et al*., *Science* **293**, 834 (2001); published online 12 July 2001 (10.1126/science.1062961).
35. A. A. Aravin *et al*., *Curr. Biol.* **11**, 1017 (2001).
36. L. Cerutti, N. Mian, A. Bateman, *Trends Biochem. Sci.* **25**, 481 (2000).

37. We thank E. Bernstein, A. Denli, and D. Conklin for critical reading of the manuscript. S.M.H. is a visiting scientist at CSHL from Genetica Inc. A.A.C. is a George A. and Marjorie H. Anderson Fellow of the Watson School of Biological Sciences and is a predoctoral fellow of the Howard Hughes Medical Institute. Supported in part by NIH grant RO1-GM62534 (G.J.H.) and by a grant from Genetica Inc. G.J.H. is a Rita Allen Foundation scholar.

3 July 2001; accepted 11 July 2001

Transitions in Distinct Histone H3 Methylation Patterns at the Heterochromatin Domain Boundaries

Ken-ichi Noma,[1] C. David Allis,[2] Shiv I. S. Grewal[1]*

Eukaryotic genomes are organized into discrete structural and functional chromatin domains. Here, we show that distinct site-specific histone H3 methylation patterns define euchromatic and heterochromatic chromosomal domains within a 47-kilobase region of the mating-type locus in fission yeast. H3 methylated at lysine 9 (H3 Lys^9), and its interacting Swi6 protein, are strictly localized to a 20-kilobase silent heterochromatic interval. In contrast, H3 methylated at lysine 4 (H3 Lys^4) is specific to the surrounding euchromatic regions. Two inverted repeats flanking the silent interval serve as boundary elements to mark the borders between heterochromatin and euchromatin. Deletions of these boundary elements lead to spreading of H3 Lys^9 methylation and Swi6 into neighboring sequences. Furthermore, the H3 Lys^9 methylation and corresponding heterochromatin-associated complexes prevent H3 Lys^4 methylation in the silent domain.

In eukaryotes, chromosomes are partitioned into structurally and functionally distinct regions that help to separate independently regulated parts of the genome (*1, 2*). Specialized DNA elements, known as insulators or boundary elements, have been suggested to mark the borders between adjacent chromatin domains and to act as barriers against the effects of enhancer and silencer elements from neighboring regions (*3–5*). The best characterized example of such long-range chromatin effects comes from studies of po-

sition effect variegation, where chromosomal rearrangements of heterochromatin near or into areas of euchromatin result in the stable epigenetic silencing of these regions (*6*–*8*). The mechanism that prevents the spreading of heterochromatin into euchromatin in a natural chromosomal context is not well understood, but recent studies suggest that boundary elements may be involved (*9, 10*).

In fission yeast, the mating-type region contains three linked loci called *mat1*, *mat2*, and *mat3* (Fig. 1). In contrast to the transcriptionally active *mat1* locus, which determines the mating type of the cell, the *mat2* and *mat3* loci and the interval between them, known as the *K*-region, are subject to heterochromatin-mediated silencing and recombinational suppression (*11*–*13*). Although silencing is thought to extend into the *L*-region, the interval between *mat1* and *mat2*, the exact boundaries between heterochromatin and euchromatin within this region are unknown (*14*). Recent in vivo evidence shows that the enzymatic methylation of Lys^9 of histone H3 by Clr4 is required for localization of Swi6, a homolog of *Drosophila* HP1, and plays a critical and highly conserved role in heterochromatin assembly (*15, 16*).

To determine the exact locations of heterochromatin within the *mat* locus and to address whether boundary elements flank the silent domain, we created a 47-kb high-resolution map by means of chromatin immunoprecipitation (ChIP) (*17*) with the polymerase chain reaction (PCR). We designed primers to amplify overlapping fragments of ~0.5 to 0.65 kb from the entire *mat* region. To amplify a part of the *K*-region well known to exhibit homology to centromeric repeats (*11*) (Fig. 1A), we selected primers from areas containing segmental insertions or substitutions, and we confirmed their specificity by using genomic DNA from a strain carrying *mat2/3* region deletion. These primer sets were used in quantitative PCR on DNA prepared either from immunoprecipitated chromatin fractions or from whole-cell crude extracts used as an input control. To account for differences in loading or the variance in amplification by different primer sets, we used multiplex PCR to normalize the relative enrichment of the *mat* sequences to the *act1* PCR product (Fig. 1).

The data show that H3 Lys^9 methylation and Swi6 were both preferentially enriched throughout a 20-kb region of DNA that included and extended past the *mat2/3* interval (Figs. 1A and 2). Unexpectedly, we observed a marked decrease in H3 Lys^9 methylation and Swi6 localization on both sides of the *mat2/3* interval, which coincided precisely with two 2-kb identical inverted repeats unique to the *mat* locus (named IR-L and IR-R, respectively, for inverted repeat left and right) (Figs. 1A and 2). Interestingly, H3 Lys^9 methylation and Swi6 were enriched at IR-L and IR-R but were not detected outside these repeats in surrounding euchromatic regions. Consistent with these results, expression of the marker genes inserted outside the IR-L toward *mat1* was unaffected, but severe repression was observed on the other side (*7, 14*) (see also Fig. 1A). Together, these data suggest that the IR-L and IR-R repeats may serve as boundaries of the silent heterochromatin domain at the *mat2/3* interval.

[1]Cold Spring Harbor Laboratory, Post Office Box 100, Cold Spring Harbor, NY 11724, USA. [2]Department of Biochemistry and Molecular Genetics, University of Virginia Health Science Center, Charlottesville, VA 22908, USA.

*To whom correspondence should be addressed. E-mail: grewal@cshl.org

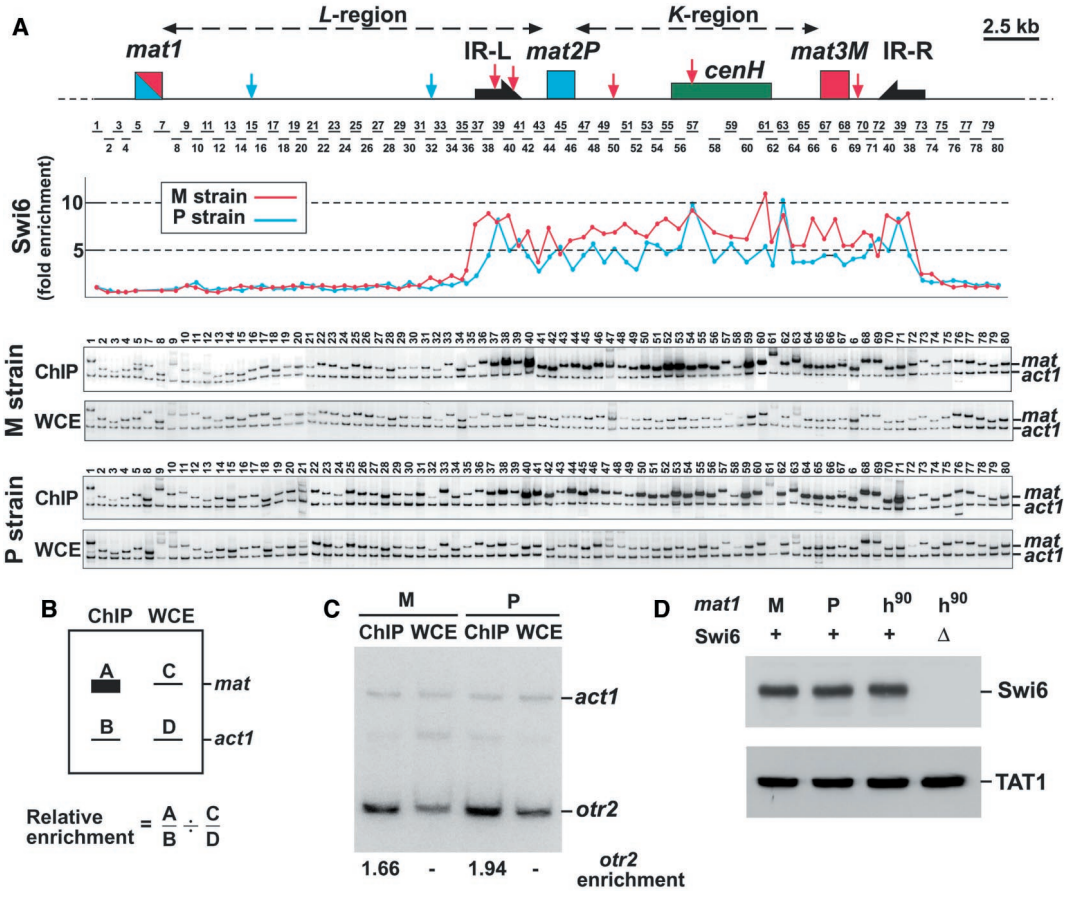

Fig. 1. High-resolution mapping of Swi6 protein levels at the mating-type region of stable *M* and *P* strains. (**A**) A physical map of the mating-type region is shown (top). IR-L and IR-R inverted repeats residing on both sides of the *mat2/3* interval are shown as black arrows. The green box represents a part of the *K*-region, *cenH*, sharing homology to centromeric repeats. Red or blue vertical arrows indicate location of marker gene insertions showing repressed or expressed state, respectively (*11, 13, 14*). ChIP analyses with antibody to Swi6 (*7*) were used to measure Swi6 levels throughout the *mat* locus. DNA isolated from immunoprecipitated chromatin (ChIP) or whole-cell crude extracts (WCE) was subjected to multiplex PCR to amplify DNA fragments from the *mat* locus, indicated by bars (1 to 80), as well as an *act1* fragment serving as an internal amplification control. PCR fragments were resolved on a polyacrylamide gel and then quantified using a phosphoimager. (**B**) Relative precipitated enrichments of *mat* sequences were calculated; quantitation of these results is plotted in alignment with the map of the *mat* locus. (**C**) The levels of Swi6 at a centromeric (*otr2*) repeat in *M* and *P* cells. DNA fractions from ChIP analyses of Swi6 levels at *mat* were analyzed for enrichment of *otr2* sequences using multiplex PCR. (**D**) Comparison of Swi6 protein levels in different mating-type backgrounds, as assessed by Western blot analysis using antibody to Swi6 (top panel) or antibody to TAT1 for loading control (bottom panel) on whole-cell protein extracts from stable *M, P*, and switching-competent h^{90} cells or *swi6*Δ strain.

Silencing at the mating-type region in *mat1-P* cells is less stringently controlled than in *mat1-M* cells (*14*), which suggests that the *P* and *M* cells might differ in their chromatin organization at the *mat* locus. Comparison between nonswitching *mat1-M* and *mat1-P* strains using ChIP analysis revealed that *P* cells contain relatively lower levels of Swi6 throughout almost the entire *mat2/3* interval (Fig. 1A). The difference in Swi6 localization appears to be limited to the *mat* locus, because no such differences in Swi6 levels were observed at centromeric repeat sequences of *M* and *P* cells (Fig. 1C) and equal amounts of Swi6 protein were present in each cell type (Fig. 1D). Interestingly, ChIP analysis revealed no clear difference in H3 Lys^9 methylation between the *P* and *M* mating-type cells (Fig. 2). This suggested that additional factors, perhaps the information encoded by *mat1-M* or *-P* loci, might account for these differences in Swi6 localization.

According to the histone code hypothesis, different posttranslational modifications of histones may have distinct biological implications (*18, 19*). In contrast to H3 Lys^9, methylation of

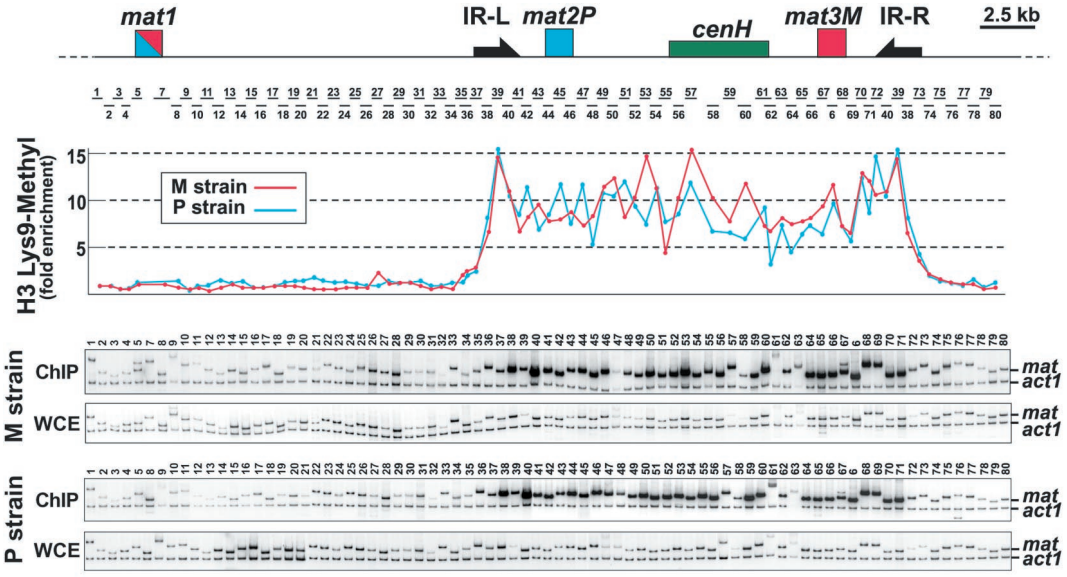

Fig. 2. Distribution of H3 Lys^9 methylation across the *mat* locus. Results from the ChIP analyses with an antibody to H3 Lys^9-methyl (*15*) are presented in alignment with the map of the *mat* locus. Quantitative measurements of H3 Lys^9 methylation levels throughout the *mat* locus were carried out as described in Fig. 1.

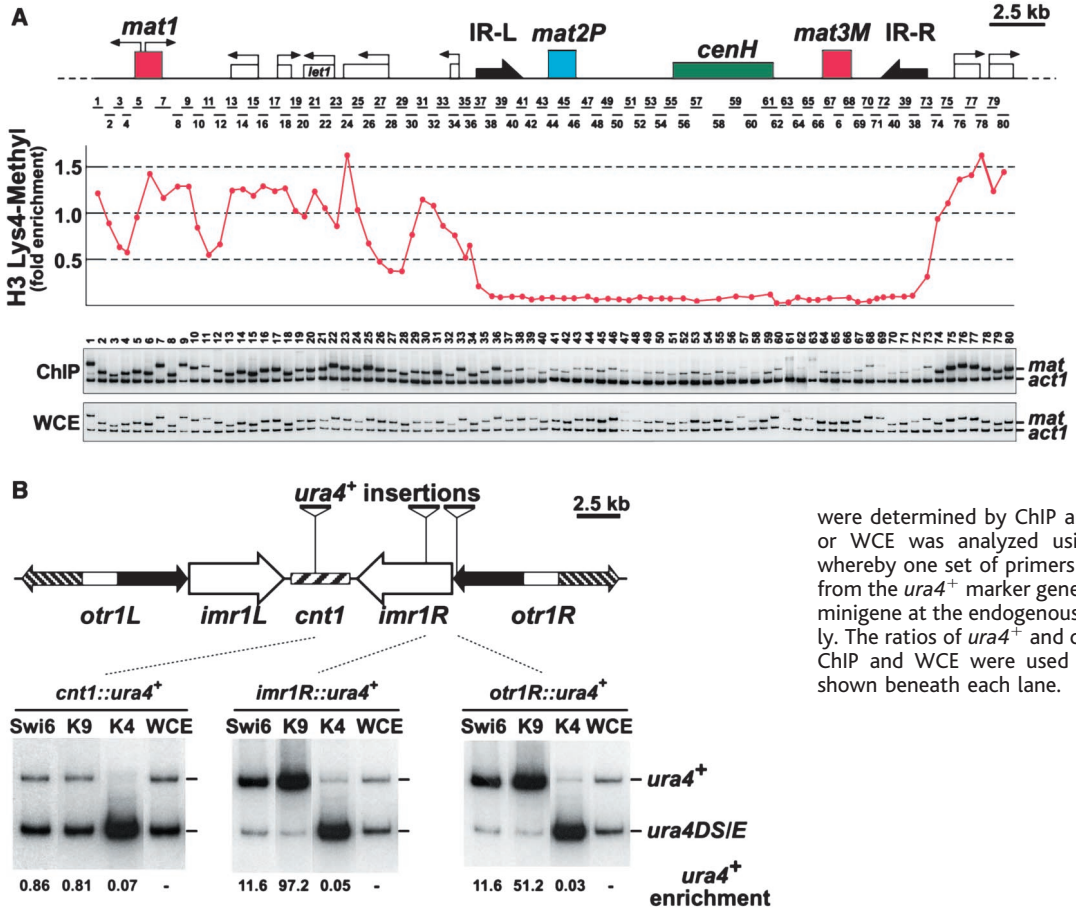

Fig. 3. Analysis of H3 Lys^4 methylation at the *mat* and *cen* loci. (**A**) Localization of H3 Lys^4 methylation at the *mat* locus. The physical map of the mating-type region indicating locations of the open reading frames (ORFs), including an essential *let1*$^+$ gene, are indicated (top). Results from ChIP analysis with antibody to H3 Lys^4-methyl (Upstate Biotechnology) are shown (bottom). Quantitation of H3 Lys^4 methylation levels at *mat*, relative to *act1* locus, is plotted. (**B**) Schematic representation of *cen1* and the corresponding *ura4*$^+$ insertion sites (top). Levels of Swi6 and Lys^4 (K4) or Lys^9 (K9) methylation of H3 at the three insertion sites were determined by ChIP analyses (bottom). DNA from ChIP or WCE was analyzed using a competitive PCR strategy, whereby one set of primers amplifies different-sized products from the *ura4*$^+$ marker gene at *cen1* and the control *ura4DS/E* minigene at the endogenous euchromatic location, respectively. The ratios of *ura4*$^+$ and control *ura4DS/E* signals present in ChIP and WCE were used to calculate relative enrichment, shown beneath each lane.

H3 Lys^4 is associated with transcriptionally active regions in *Tetrahymena* (*20*). To compare these two sites, we next sought to map at high resolution the H3 Lys^4 methylation pattern across the same locus. ChIP analysis revealed that H3 Lys^4 methylation was enriched at transcriptionally competent regions surrounding the inverted repeats, as well as at the *act1* locus, but no enrichment was observed throughout the heterochromatic region flanked by the IR-L and IR-R elements (Fig. 3A). The levels of H3 Lys^4 methylation are higher in the regions containing genes than in intergenic regions (Fig. 3A). These findings suggest that H3 Lys^4 methylation is associated with the euchromatic regions of the genome but is lacking at the heterochromatic domains. Indeed, ChIP analysis showed that H3 Lys^4 methylation was absent at the *ura4*$^+$ marker inserted within the transcriptionally repressed centromeric (*otr* and *imr*) repeats, but was enriched at the *ura4DS/E* endogenous euchromatic location (Fig. 3B). The lack of H3 Lys^4 methylation at the *otr* and *imr* locations coincides with the presence of H3 Lys^9 methylation and Swi6 (Fig. 3B). As expected, H3 Lys^4 methylation was not detected at the central core (*cnt*) region, where the histone H3 variant CENP-A is localized (*21*). Although the biological significance of H3 Lys^4 methylation is not yet clear, it is possible that this histone modification may serve to recruit transcriptional coactivators, similar to arginine methylation of histone H4 (*22*). Together, these results further suggest that the IR-L and IR-R repeats define the borders between euchromatin and heterochromatin, and that distinctive patterns of H3 methylation exist on opposite sides of these putative boundary elements.

If IR-L and IR-R repeats are bona fide boundary elements, deletions of either repeat should result in the spreading of heterochromatin into neighboring regions. For this purpose, strains containing a deletion of either IR-L or IR-R were constructed (*23*). Because spreading of heterochromatin is stochastic and depends on dosage of chromatin proteins, we used strains carrying three copies of *swi6*$^+$, which is known to enhance silencing at the *mat*

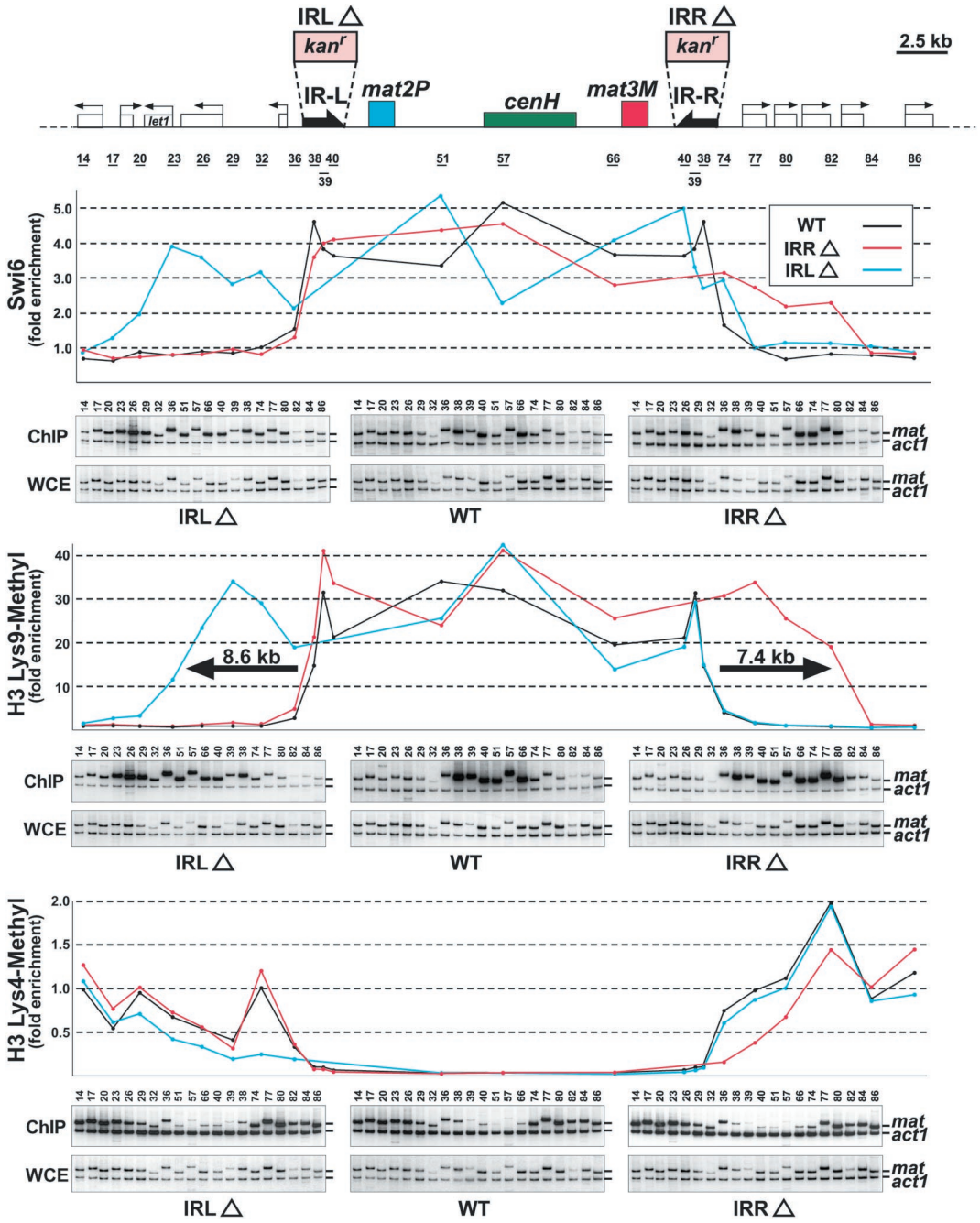

Fig. 4. Deletion of IR-L or IR-R causes spreading of heterochromatin into flanking regions. Three strains (WT, IR-LΔ, and IR-RΔ) were used. Results from ChIP analyses with antibodies to Swi6, H3 Lys^9-methyl, or H3 Lys^4-methyl are shown aligned with the map of the *mat2/3* interval and surrounding regions. Numbered bars below the map indicate PCR fragments analyzed in each ChIP assay. Thick arrows indicate direction and distance of heterochromatin spreading that was caused by IR-LΔ or IR-RΔ.

locus (*7*). Remarkably, the IR-L deletion resulted in the spreading of both H3 Lys^9 methylation and Swi6 localization to more than 8 kb of the adjoining *L*-region, whereas no spreading was observed in IR-L$^+$ cells (Fig. 4). Furthermore, the spreading of heterochromatin was associated with a decrease in H3 Lys^4 methylation levels in the *L*-region. The IR-L deletion also caused growth defects, most likely due to the spreading of heterochromatin into the essential *let1*$^+$ gene. Spreading of H3 Lys^9 methylation and Swi6, and a concomitant decrease in H3 Lys^4 methylation, was also observed in the IR-R deletion strain (Fig. 4), indicating that these repeats are indeed boundary elements that function to prevent heterochromatic spreading into neighboring euchromatic regions.

Recently, it was suggested that insulators may pair in cis to form chromatin loops within the nucleus (*24*–*26*). Therefore, it was of interest to determine whether deletion of IR-L would affect IR-R boundary function, or vice versa. Although it remains a formal possibility that the IR-R or IR-L elements may interact with each other, we found that these repeat elements can operate independently of each other in preventing the spreading of Swi6 and H3 Lys^9 methylation to adjacent sequences on their respective sides (Fig. 4). That is, IR-LΔ did not affect IR-R boundary activity, and vice versa.

The results presented above indicate that the presence of repressive heterochromatin complexes at the *mat2/3* interval may prevent H3 Lys^4 methylation or, alternatively, that H3 Lys^9 methylation may directly inhibit H3 Lys^4 methylation. To test this, we performed ChIP analysis on the *Kint2::ura4*$^+$ marker gene inserted at the *K*-region (Fig. 5A). In a *swi6-115* mutant strain, which results in defects in Swi6 localization and loss of silencing, H3 Lys^9 methylation was unchanged; however, there was an observed increase in H3 Lys^4 methylation relative to wild-type background cells. Deletion of *clr4*, the histone methyltransferase responsible for H3 Lys^9 methylation, resulted in a marked decrease of both H3 Lys^9 methylation and Swi6 localization but a much more pronounced increase in H3 Lys^4 methylation relative to the wild type and *swi6-115* strains. Taken together, these data indicate that H3 Lys^9 methylation, in combination with heterochromatin-associated proteins such as Swi6, prevents H3 Lys^4 methylation at the *mat2/3* region.

Collectively, these results suggest that methylation of H3 at Lys^4 or Lys^9 is reciprocally associated with euchromatic and heterochromatic regions, respectively. We also provide direct evidence that the boundary elements that define the borders between euchromatin and heterochromatin protect against the encroachment of heterochromatin signals into neighboring euchromatic regions. Boundary or insulator sequences have been suggested to govern subnuclear organization of DNA (*24*). In this regard, we find that the *mat* locus is localized near the nuclear periphery (*27*). We hypothesize that the higher order chromatin organization at the *mat2/3* interval involves (i) the methylation of H3 Lys^9 and the subsequent localization of heterochromatin-associated proteins to establish a primary level of organization, and (ii) the binding of specialized proteins to boundary elements that then tether the *mat* locus to the nuclear periphery (Fig. 5B). This specialized chromatin organization results in silencing and recombination suppression, and is likely to promote long-range interaction between *mat1* and the opposite mating-type donor locus, which is required for efficient switching (*11, 28*). Further characterization of the boundary elements and their role in preserving distinct chromatin configurations will help us better understand the higher order organization of chromosomes.

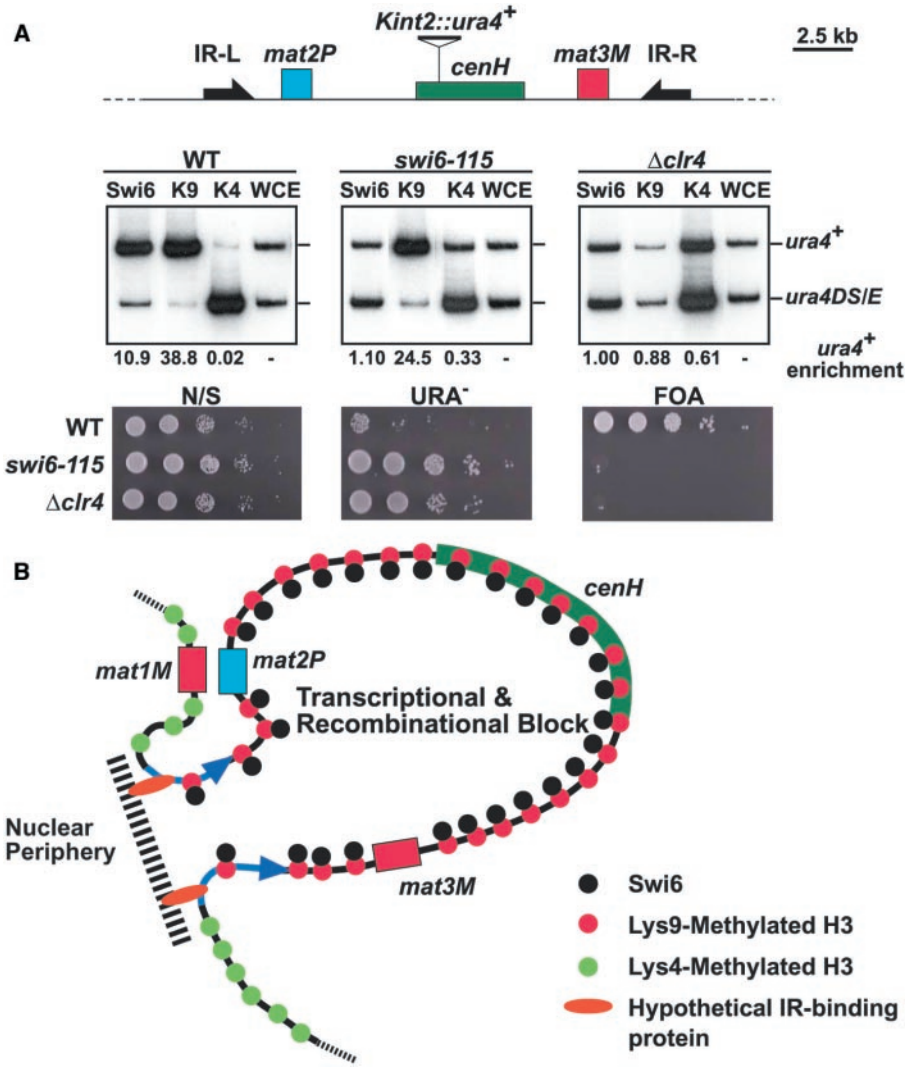

Fig. 5. (**A**) Effect of H3 Lys^9 methylation and heterochromatin on H3 Lys^4 methylation at *mat2/3* region. The physical map of the mating-type locus indicates the *Kint2::ura4*$^+$ insertion site (top). ChIP with competitive PCR analyses, as described in Fig. 3, was used to measure the effect of mutations in *swi6* (*swi6-115*) or *clr4* (Δ*clr4*) on Lys^4 (K4) or Lys^9 (K9) methylation of H3 and Swi6 at *Kint2::ura4*$^+$. Serial dilutions of indicated cultures were plated onto nonselective (N/S), medium lacking uracil (URA$^-$), or 5-fluoroorotic acid (FOA) medium to assay *ura4*$^+$ expression (bottom). (**B**) Schematic model showing a proposed higher order chromatin organization at the *mat* locus. The IR-L and IR-R boundary elements (blue arrows) prohibit the spreading of Swi6 and H3 Lys^9 methylation to the flanking euchromatic regions. In addition, we hypothesize that these elements might also tether the *mat* locus to nuclear periphery, thereby creating a specialized domain.

References and Notes

1. F. L. Sun, S. C. Elgin, *Cell* **99**, 459 (1999).
2. A. C. Bell, A. G. West, G. Felsenfeld, *Science* **291**, 447 (2001).
3. R. Kellum, P. Schedl, *Cell* **64**, 941 (1991).
4. A. C. Bell, G. Felsenfeld, *Nature* **405**, 482 (2000).
5. A. T. Hark *et al.*, *Nature* **405**, 486 (2000).
6. L. Wallrath, *Curr. Opin. Genet. Dev.* **8**, 147 (1998).
7. J. Nakayama, A. J. S. Klar, S. I. S. Grewal, *Cell* **101**, 307 (2000).

8. J. F. Partridge, B. Borgstrom, R. C. Allshire, *Genes Dev.* **14**, 783 (2000).
9. X. Bi, J. R. Broach, *Curr. Opin. Genet. Dev.* **11**, 199 (2001).
10. D. Donze, C. R. Adams, J. Rine, R. T. Kamakaka, *Genes Dev.* **13**, 698 (1999).
11. S. I. S. Grewal, A. J. S. Klar, *Genetics* **146**, 1221 (1997).
12. S. I. S. Grewal, *J. Cell. Physiol.* **184**, 311 (2000).
13. G. Thon, A. Cohen, A. J. S. Klar, *Genetics* **138**, 29 (1994).
14. N. Ayoub, I. Goldshmidt, A. Cohen, *Genetics* **152**, 495 (1999).
15. J. Nakayama, J. C. Rice, B. D. Strahl, C. D. Allis, S. I. S. Grewal, *Science* **292**, 110 (2001).
16. A. J. Bannister *et al.*, *Nature* **410**, 120 (2001).
17. Chromatin immunoprecipitations were performed essentially as described (*7, 8*). Fission yeast cells grown at 32°C in yeast extract adenine (YEA) medium (5×10^8 cells at 10^7 cells/ml for each reaction) were shifted to 18°C for 2 hours before 30-min fixation in 3% paraformaldehyde, and then were used to prepare soluble chromatin. Chromatin fractions were fragmented to ~0.5- to 0.8-kb DNA fragments before immunoprecipitation using antibodies to Swi6, H3 Lys^9-methyl, or H3 Lys^4-methyl. DNAs recovered from immunoprecipitated chromatin fractions or from whole-cell crude extracts were subjected to PCR analyses (94°C, 30 s; 55°C, 30 s; 72°C, 1 min; 30 cycles). PCR products were labeled by including 0.25 μl of [α-^{32}P]deoxycytidine triphosphate (10 mCi/ml) in each reaction; they were separated on a 4% polyacrylamide gel, and band intensities were quantified using a Fuji phosphoimager.
18. B. D. Strahl, C. D. Allis, *Nature* **403**, 41 (2000).
19. T. Jenuwein, C. D. Allis, *Science* **293**, 1074 (2001).
20. B. D. Strahl, R. Ohba, R. G. Cook, C. D. Allis, *Proc. Natl. Acad. Sci. U.S.A.* **96**, 14967 (1999).
21. K. Takahashi, E. S. Chen, M. Yanagida, *Science* **288**, 2215 (2000).
22. H. Wang *et al.*, *Science* **293**, 853 (2001); published online 31 May 2001 (10.1126/science.1060781).
23. Because of recombination block in the silent mating-type region, replacement of IR-L or IR-R elements with *kan*^{r} was performed in the *swi6* mutant background, which allows recombination in this region. The DNA fragment containing the marker gene flanked by sequence corresponding to the 5′ or 3′ sequence of the site of integration was gel-purified and used for transformation to construct IR-RΔ and IR-LΔ strains. PCR and Southern analyses were used to confirm replacements. Genetic crosses were used to obtain *swi6*$^+$ derivatives of the above strains. Deletions did not have a detectable effect on silencing of *ura4*$^+$ (*Kint2::ura4*$^+$) inserted at the *K*-region.
24. T. I. Gerasimova, K. Byrd, V. G. Corces, *Mol. Cell* **6**, 1025 (2000).
25. H. N. Cai, P. Shen, *Science* **291**, 493 (2001).
26. E. Muravyova *et al.*, *Science* **291**, 495 (2001).
27. J. Nakayama, S. I. S. Grewal, unpublished data.
28. G. Thon, A. J. S. Klar, *Genetics* **134**, 1045 (1993).
29. We thank J. Rice and E. Heard for comments on the manuscript, J. Nakayama for helpful discussions and boundary element sequences, and G. Xiao, Y. Tsukamoto, R. Rice, and M. A. Jelnick for technical help. Supported in part by a grant from Ellison Medical Foundation (S.I.S.G.) and by NIH grants GM59772 (S.I.S.G.) and GM53512 (C.D.A.).

6 July 2001; accepted 17 July 2001

Crystal Structure of a Neutralizing Human IgG Against HIV-1: A Template for Vaccine Design

Erica Ollmann Saphire,[1] Paul W. H. I. Parren,[2] Ralph Pantophlet,[2] Michael B. Zwick,[2] Garrett M. Morris,[1] Pauline M. Rudd,[4] Raymond A. Dwek,[4] Robyn L. Stanfield,[1] Dennis R. Burton,[1,2]* Ian A. Wilson[1,3]*

We present the crystal structure at 2.7 angstrom resolution of the human antibody IgG1 b12. Antibody b12 recognizes the CD4-binding site of human immunodeficiency virus–1 (HIV-1) gp120 and is one of only two known antibodies against gp120 capable of broad and potent neutralization of primary HIV-1 isolates. A key feature of the antibody-combining site is the protruding, finger-like long CDR H3 that can penetrate the recessed CD4-binding site of gp120. A docking model of b12 and gp120 reveals severe structural constraints that explain the extraordinary challenge in eliciting effective neutralizing antibodies similar to b12. The structure, together with mutagenesis studies, provides a rationale for the extensive cross-reactivity of b12 and a valuable framework for the design of HIV-1 vaccines capable of eliciting b12-like activity.

HIV-1 vaccine development is greatly hindered by the extreme difficulty in eliciting a neutralizing antibody response to the virus (*1–3*). However, three human monoclonal antibodies have been identified that can efficiently neutralize a broad array of primary isolates of HIV-1 in vitro (*4*) and can protect against viral challenge in vivo (*5–9*). Antibody 2F5 (*10*) reacts with gp41, whereas 2G12 (*11*) and b12 (*12*) react with independent epitopes on gp120. Elucidation of the epitopes recognized by these antibodies may offer valuable insights into the design of antigens capable of eliciting a protective antibody response.

Antibody b12 was identified from a combinatorial phage display library developed from bone marrow donated by a 31-year-old homosexual male who had been seropositive, but without symptoms, for 6 years (*12*). This antibody recognizes a highly conserved epitope overlapping the CD4-binding region of gp120, which accounts for its broad recognition of different HIV-1 isolates. Antibody b12 neutralizes about 75% of clade B primary viruses and a similar, or somewhat lesser, proportion of other clades (*12*, *13*). In addition, b12 can protect hu-PBL-SCID mice (*5*) and macaques (*7*) from viral challenge. This combination of potency and broad specificity suggests that the b12 epitope on gp120 may be a particularly effective target for vaccine design.

The b12 IgG1κ was expressed in CHO cells, purified, and crystallized as previously described (*14*). The crystal structure of the intact IgG1 was determined at 2.7 Å resolution through an exhaustive molecular replacement (MR) search using more than 100 individual Fc and Fab search models (*14*). The highly mobile hinge regions connecting the Fabs to the Fc domains were interpretable after extensive rebuilding, refinement, and density modification (Table 1). Only three residues of the upper hinge of one heavy chain, seven residues of a frequently disordered surface loop of one Fab C_H1 domain (residues 128 to 135), and three COOH-terminal residues from one Fc are disordered.

The IgG structure is highly asymmetric (Fig. 1) and can be considered a "snapshot" of the broad range of conformations available in solution. The overall shape is between a Y and a T, with a 143° angle between the major axes of the two Fabs (*15*). The IgG spans 171 Å from the apex of one antigen-binding site to the other. The Fc region is twisted nearly perpendicularly to the planes of the Fabs and shifted some 32 Å from the central dyad relating the two Fabs, so that it packs into the space beneath only one of the Fabs (Fig. 1).

The hinge regions form extended structures with some conformational variation in torsion angles between the two chains, reflecting the different relative placement and environment of the two Fabs relative to the Fc domain. One upper hinge forms a spiral arrangement similar to a partially unwound helix; the other forms an extended turn as the polypeptide chain reverses direction to connect the Fab to the Fc. The core hinge region contains two adjacent pairs of cysteine residues, but only one disulfide is ob-

[1]Department of Molecular Biology, [2]Department of Immunology, [3]The Skaggs Institute for Chemical Biology, The Scripps Research Institute, 10550 North Torrey Pines Road, La Jolla, CA 92037, USA. [4]Department of Biochemistry, University of Oxford, The Oxford Glycobiology Institute, South Parks Road, Oxford OX1 3QU, UK.

*To whom correspondence should be addressed. E-mail: wilson@scripps.edu, burton@scripps.edu